1-1-2016

Role of Micro-CT in the Visualization, Measurement, and Quantification of Bone Structure in Osteogenesis Imperfecta

Robert C. Molthen
Marquette University, robert.molthen@marquette.edu

John Jameson
Marquette University, john.jameson@marquette.edu

Carolyne Albert
Marquette University, carolyne.albert@marquette.edu

Peter Smith
Schriners Hospitals for Children, Chicago, IL

Gerald F. Harris
Marquette University, gerald.harris@marquette.edu

Published version. *Transitional Care in Osteogenesis Imperfecta: Advances in biology, Technology, and Clinical Practice*, (2016): pp. 195-216. Publisher link.

12 ROLE OF MICRO-CT IN THE VISUALIZATION, MEASUREMENT, AND QUANTIFICATION OF BONE STRUCTURE IN OSTEOGENESIS IMPERFECTA

Robert Molthen, Ph.D.[1]
John Jameson, Ph.D.[1,2]
Carolyne Albert, Ph.D.[1,3]
Peter Smith, M.D.[3]
Gerald Harris, Ph.D., P.E.[1,3]

[1] Orthopaedic and Rehabilitation Engineering Center (OREC), Marquette University and The Medical College of Wisconsin, Milwaukee, WI [2]
[2] Mayo Clinic, Department of Physiology and Biomedical Engineering, Rochester, MN
[3] Shriners Hospitals for Children, Chicago, IL

INTRODUCTION

Even though bone and skeletal disorders are primary symptoms of osteogenesis imperfecta (OI), relatively few attempts have been made to estimate OI bone morphometric indices, determine how OI weakens the osseous tissue architecture, or quantitatively stratify risk of fracture. Currently, there is little biomechanical data on OI bone. The majority of characterization studies have used simple measures of bone quantity, such as bone mineral density (BMD), to provide an estimate of bone integrity. However, the mechanical properties and performance of bone depend on many factors in addition to the quantity of bone present including the quality of existing material and the three-dimensional trabecular architecture.[1-3] New methods of analysis, such as imaging, in particular micro-Computed Tomography (micro-CT), offer a novel, non-destructive technique for analyzing bone specimens and developing better biomechanical models for determining fracture risk assessment and clinical management approaches.[1,4-6]

Micro-CT Instrumentation and Specimen Scanning

Micro-CT offers the capacity to three-dimensionally (3-D) image bone structures down to the trabecular level and smaller. In order to capture and properly quantify trabecular morphology, micro-CT imaging systems must have the ability to resolve features in the tens of microns range or smaller. Currently, few imaging systems with this capability, especially those used for *in vivo* scanning, have been designed or are available on the market. More so, virtually none are approved and available for doing *in vivo* studies in humans. In recent years, several instrumentation manufacturers have introduced micro-CT imaging systems primarily for research applications and 'non-destructive' analysis of excised or isolated samples, in some cases under *in vitro* conditions. Many of the imaging systems provide more than acceptable results when scanning bone, since its material composition supplies relatively high contrast within the energy range of typical X-ray sources implemented. All commercially available imaging systems employ polychromatic X-ray sources with wide energy spectrums (at least tens of keVs). Since the attenuation coefficient of materials being studied is a strong function of the incident X-ray energy, there are inherent artifacts, such as beam hardening (caused by non-uniform attenuation of photons with those in the lower energy ranges being selectively filtered out), in the resulting images. A polychromatic energy source combined with a detector that cannot discriminate the energy of incident photons also prohibits performing material composition. Select systems have the ability to resolve structures as small as several microns, although there is generally a trade-off in increased scan time as resolution increases. For example, high-resolution scans (< 10 microns) may take a number of hours to complete for a sample that is only a few centimeters long. In addition, depending on spatial resolution, grayscale resolution (i.e., the bit depth of the individual volume element or voxel), sample size, and field of view required or obtained, the resultant data sets can easily be in excess of several gigabytes. These large data set sizes evoke their own unique challenges such as file storage, file management, and data analysis. As a result, in depth guidelines for the assessment of bone microstructure in rodents using micro-CT have been developed.[7]

Data Analysis

Simple dimensional measurements such as lengths, cross sectional areas, cortical thickness, etc. can be easily determined with most standard image analysis software as long as spatial information about voxel sizes are either

embedded in the image file or input as part of the file import/loading procedure. Complex morphometric parameters analysis of micro-CT bone data is more involved and requires specialized software tools or algorithms. In addition, a preprocessing step is required where a threshold based segmentation algorithm is used to identify and isolate bone from any other materials present within the imaged volume. One automated thresholding technique often used for bone segmentation is the clustering-based Otsu method.[8] Once the image volume has been segmented the data can be binarized, such that voxels identified as 'bone' are assigned the value of 1 and all others are assigned 0, or the grayscale value of bone voxels is retained and all other voxels set to an arbitrary, non-overlapping value. Although most current bone morphometry algorithms are designed to use binary data, some novel approaches are capable of processing grayscale data.

Trabecular bone samples from vertebrae tend to be more rod-like, whereas bone from femoral head tends to be more plate-like. In trabecular bone analysis it is not appropriate to apply model assumptions often used in 2-D analysis, since the "plate-like" or "rod-like" character of trabecular bone can change both between bone samples and from one end of a volume of interest (VOI) to the other. Therefore, most contemporary 3-D analysis software is model-independent and will measure morphometric parameters directly without the need for addressing shaped-based assumption.

Bone Morphology, Morphometry, Microstructure, and Quantitative Parameters

This section describes the quantitative morphometric parameters that are typically calculated and made available by analyzing micro-CT data. Advanced CT bone imaging, formulation of morphometric parameters, and in depth discussion of their practical implementation can be found in many sources.[5,7,9-12] Here we provide a succinct overview and definitions as background. A summary of the parameters can be found in Table 1.

Table 1. Summary of bone indices.

Index	Abbreviation	Description	Standard unit
Total (Tissue) Volume	TV	Volume of volume of interest	mm^3
Bone Volume	BV	Volume of region segmented as bone	mm^3
Bone volume density	BV/TV	Ratio of BV to the TV	%
Trabecular Thickness	Tb.Th	Mean thickness of trabeculae	mm
Trabecular Spacing	Tb.Sp	Mean distance between trabeculae	mm
Trabecular Number	Tb.N	Average number of trabeculae per unit length	1/mm
Bone Surface	BS	Surface area of region segmented as bone	mm^2
Specific Bone Surface	BS/BV	Ratio of BS to the BV	1/mm
Cross Sectional Area	CSA	Area of cross sectional slice of bone specimen	mm^2
Cortical Thickness	Ct.Th	Thickness of cortical bone	mm
Tissue Mineral Density	TMD	Total mineral mass in the region segmented as bone	mg/cm^3
Bone Mineral Content	BMC	Total mineral mass in the VOI	mg
Bone Mineral Density	BMD	BMC normalized by the volume of the VOI	mg/cm^3
Connectivity Density	Conn.D	A measure of the connectivity of the trabeculae divided by TV	$1/ mm^3$
Degree of Anisotropy	DA	Length of longest divided by the shortest mean intercept length vector	*
Structure Model Index	SMI	Indicator of the structure of the trabeculae	*

* Dimensionless variable

Bone volume density, often represented as BV/TV, is one of the most common and often reported micro-CT parameters that represents the fraction of a given VOI, total volume, or tissue volume (TV) that is occupied by bone (BV) and is usually reported as a percentage value. BV/TV can be used to evaluate relative changes in bone volume present from one time point to another or before and after a given treatment, for example after treatment with common anti-resorptive drugs such as bisphosphonates.

Unfortunately, BV/TV, like many morphometrics parameters, will vary if the selected VOI is different from one scan to another or when the same data is analyzed using different VOIs. Furthermore, if another material is present in the VOI, such as metal hardware, the artifacts present will result in segmentation errors and anomalous estimation of values. Likewise, comparative analysis between samples will not be possible if different scanner settings have been used or if there are inconsistencies in specimen preparation.

Trabecular thickness (Tb.Th) and trabecular spacing (Tb.Sp) are measures of the 3-D structure of cancellous or spongy bone. As the names imply, these parameters characterize the thickness of the trabecular columns and the spacing in between, respectively. These parameters are often reported as a mean, for example mean thickness of the structure calculated as the volume weighted average of the local thicknesses. We can imagine that these scalar measures are not able to describe all structural attributes, i.e., the same value may be obtained in a case where the struts are of uniform thickness compared to one where the struts taper considerably. Therefore, it may be more useful and informative to represent the thickness and spacing parameter on a continuum for the VOI as a histogram of the values. Trabecular number (Tb.N) is taken as the inverse of the mean distance between the mid-axes of the structure to be examined. The mid-axes are assessed using a 3-D distance transformation and extracting the center points of 'non-redundant' spheres set to fill the structure completely. The mean distance is calculated as the average separation between the mid-axes and the Tb.N determined.

Bone surface (BS) and specific bone surface (BS/BV) can be calculated by tessellating or creating a two-dimensional plane using repeated geometric shapes (usually triangles) with no overlaps and no gaps utilizing the segmented portion of the image data that has been identified as bone. The typical approach to calculate these parameters is to create a polygonal mesh

that represents the surface of the object. The Volumetric Marching Cubes algorithm is usually used to place tetrahedrons (or hexahedrons) on the surface of the object.[13] A better representation of the surface is typically obtained by smoothing the mesh before summing the total area of all polygons to estimate the bone surface (BS) of the identified structure. An additional benefit to creating these meshes is that they can be used as input files for finite element simulations. The BV computation becomes the volume within the tessellated surface and the BS/BV follows as a measure for the bone surface per given bone volume. This parameter is used because it provides a measure of how many bone-lining cells cover a given volume of bone.

Bone mineral content (BMC) is the total of all mineral mass in a VOI or the amount of mineral matter within the sampled volume. Bone mineral density (BMD) is derived by normalizing BMC by the volume of the VOI. Tissue mineral density (TMD) is the total mineral mass in the region within the VOI that has been segmented as bone. Whereas BMD measures the average quantity of bone mass in a representative volume, TMD measures the density of the bone material in that volume.

Simple dimensional parameters that are used to quantify cortical bone include cross-sectional area (CSA), which determines the area of cortical bone contained within a selected cross-section defined for analysis and cortical thickness (Ct.Th), the thickness of the cortex measured in a region at a selected cross-section.

Several other parameters have been used to characterize cancellous bone. Connectivity density (Eu.Conn.D or Conn.D) exploits Euler analysis and provides a measure of the connectivity of the trabecular network, indicating the number of redundant connections between trabecular structures per unit volume. The degree of anisotropy (DA) provides a measure of the directional dependence of trabeculae and is equal to the length of the longest divided by shortest mean intercept length vector (DA is 1 for ideally isotropic conditions, while this number is increasingly larger when the bone is more anisotropic). Finally, structure model index (*SMI*) describes the degree to which the trabecular network follows common plate-like or rod-like structural models (SMI will be 0 for parallel plates and 3 for cylindrical rods).[14]

MOUSE MODEL OF OI BONE MORPHOLOGY

OI is a genetic bone fragility syndrome commonly characterized by mutations in the genes that code for type I collagen and its associated structural proteins. Type I collagen and hydroxyapatite (HA) are the most prevalent organic and inorganic components in bone, respectively, and these components contribute significantly to its mechanical properties.[15] Most symptoms of OI can be attributed to altered collagen synthesis and assembly. Clinically, OI patients are currently classified into eight groups, Type III being the most severe form compatible with life. Due to limited availability and the small size of excised human OI specimens, animal models have been developed for research purposes. Murine models, typically with defective collagen synthesis abnormalities, have become standard surrogates for research in OI.[16-18] One common mouse model of Type III OI is the homozygous oim B6C3Fe a/a-Col1a2oim/J strain (oim/oim).[19] Although a number of studies have addressed determining bone morphometric parameters using micro-computed tomography (micro-CT),[1,9-12,20] the goal of the work presented here was to gather baseline data and validate a micro-CT system for the evaluation of murine models of OI and human OI bone samples.

Methods

Animals

All studies were performed under approval of an Institutional (Medical College of Wisconsin and Zablocki Veterans Affairs Medical Center) Animal Care and Use Committee (IACUC) protocol. Mice were obtained from Jackson Laboratory (Bar Harbor, ME). Ten male mice were anesthetized and euthanized, after which five oim/oim and five wild-type (+/+) femora were harvested and fresh frozen at -70°C until micro-CT evaluation. Average ages of the oim/oim and +/+ mice at tissue dissection were 9 and 10 weeks, respectively.

Imaging

Scans were performed using a custom-built micro-CT system designed and developed at the Zablocki Veterans Affairs Medical Center (Milwaukee, WI). The system has a simple cone beam geometry composed of a FeinFocus 100.50 X-ray source (3-μm focal spot; Comet North America, Stamford, CT), an AI-5830-HP image intensifier (North American Imaging, Camarillo, CA) coupled to a Silicon Mountain Design SMD1M-15 CCD camera (Teledyne

DALSA, Billerica, MA), and a specimen micromanipulator stage, mounted on a precision rail as described in previous reports.[21-23] Femora were thawed, placed in 1.5-mL Eppendorf tubes filled with saline, mounted on the specimen stage, and scanned using continuous rotation (33 kVp, 242 μA, 7-frame average) at two magnifications. Reconstructions were performed using a standard Feldkamp reconstruction algorithm,[24] with resulting isotropic voxel sizes of 17 and 34 μm, corresponding to high and low magnification, respectively.

Analysis

Image visualization, VOI selection, and morphometric parameter estimation were performed using ImageJ (v1.42; NIH) and MicroView (v2.1.2; GE Healthcare, Waukesha, WI). VOIs in each specimen were determined and analyzed for several locations in cortical and trabecular bone. Femoral length was measured using the line tool within MicroView. Longitudinal cortical regions were selected from the low-magnification scans. These cortical VOIs extended distally 2.5 mm from the femoral midpoint and were used to measure CSA and Ct.Th. Measurements of Ct.Th were made at the mid-diaphysis and each value reported is an average of 10 measurements taken all around the cross-section. Cylindrical shaped trabecular regions were isolated from high-magnification data volumes, proximal and adjacent to the distal femoral growth plate, extending proximally 1.5 mm with a diameter of 1 mm. A local threshold (determined using MicroView's auto-threshold option) was used to segment and isolate trabecular VOIs, and these regions were subsequently evaluated for BV/TV, Tb.N, Tb.Th, and Tb.Sp.

Statistical analysis

Data from each genotype was pooled and compared for statistical significance using an unpaired student's t-test.

Results

Femoral length was not significantly different between femurs from oim/oim and wild-type mice. However, cortical and trabecular indices were generally inferior for oim/oim mice compared to controls (Table 2). Figure 1A shows an example of a surface-shaded rendering of a micro-CT image of a normal mouse femur. In Figure 1B renderings of example portions of a femur and trabecular bone ROI from a normal and oim/oim mouse are presented for visualization. The qualitative visual appearance of the oim/oim cortical cross-sectional geometry was more flattened and ellipsoidal in appearance

than seen in the wild-type mice (Figure 1B). Mid-shaft oim/oim cortices showed a 16% reduction in CSA, suggesting decreased resistance to bending loads. These observations are in agreement with findings from a previous study.[25] The oim/oim trabecular network appeared more rarefied (Figure 1B), which was confirmed by significantly reduced BV/TV and Tb.N, as well as a corresponding increase in Tb.Sp (Table 2).

Table 2. Summary of calculated bone parameters.

Genotype	Morphometric Parameters					
	CSA (mm^2)	*Ct.Th* (*mm*)	*BV/TV*	*Tb.N* (mm^{-1})	*Tb.Th* (*mm*)	*Tb.Sp* (*mm*)
Control (+/+)	0.87 ± 0.15	0.20 ± 0.03	0.25 ± 0.05	6.89 ± 1.71	0.036 ± 0.006	0.12 ± 0.04
Oim/oim	0.73 ± 0.10*	0.19 ± 0.01	0.14 ± 0.03†	3.67 ± 1.03†	0.038 ± 0.005	0.28 ± 0.09†

* $p < 0.06$ between +/+ and *oim/oim*.
† $p < 0.05$ between +/+ and *oim/oim*.

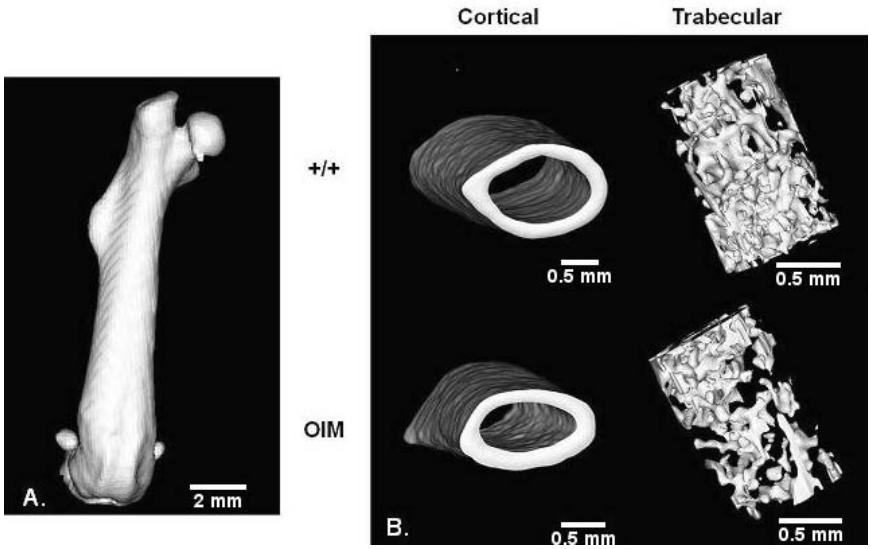

Figure 1. Representative surface-shaded renderings of mouse femora from μCT data. (A) Whole femur from a normal wild-type mouse. (B) Cortical and trabecular VOIs.

Discussion

The results support prior findings reporting that OI mice have a decrease in trabecular tissue and reduced mechanical integrity.[25,26] The resolution achieved (isotropic voxel size of 17 μm) for our trabecular analysis is sufficient for mouse bone specimens and the resulting indices estimated agreed well with values previously reported in the OI mouse literature.[25-27] The study confirms that the scanning and analysis methods employed can be applied to murine bone samples and that these techniques enable examination of differences in bone structure between OI mouse models and their wild-type counterparts.

STUDY OF HUMAN OI SAMPLES

In the clinical setting, bone mineral and structural parameters are typically determined using 2-D techniques including dual-energy X-ray absorptiometry (DEXA) and histology. Although these methods have become accepted clinical standards,[28,29] they provide only limited data and are inadequate for developing better quantitative analysis of fracture risk and therapeutic intervention. DEXA integrates mineral information into 2-D data providing only mean values across the sample volume. Three-dimensional information that may be fundamentally important to understanding bone mechanical properties is lost and the ability of DEXA alone to accurately predict fracture is questionable, especially in the growing skeleton.[30] In addition, DEXA scans subject patients to ionizing radiation, and although the radiation dose is relatively small, this raises safety concerns for OI patients who routinely undergo multiple annual X-ray scans (e.g. for fractures, deformity mapping, follow-ups, etc.). Fan et al. have used a novel nanoindentation method to characterize OI bone.[31-33] However, histological and nanoindentation evaluation require destructive excision and morphometric parameters derived from histology rely on geometric and material distribution assumptions to extrapolate 3-D properties from 2-D slides. Therefore, where conventional radiography and histological analysis has been the mainstay of fracture assessment, micro-CT may allow for a large improvement in characterizing the degree of underlying bone fragility, the progression of fracture healing, and for monitoring interventional therapies.[1-3]

Micro-CT affords straightforward 3-D analysis of BMD and bone microstructure.[34] Although high-resolution CT and micro-CT are relatively new to the clinical arena, scanners have been recently developed and made commercially available allowing examination of human limbs *in vivo* and providing qualitative and quantitative assessment of bone microstructure.[35-38] Micro-CT can be particularly useful for OI research because patients routinely undergo corrective surgeries that involve removal of small bone fragments. After establishing agreement with studies reported for murine models, we applied our methods to human OI bone specimen. The study[39] was aimed to investigate micro-CT as a method to characterize OI bone architecture in several of these excised fragments, and to compare the results to previous reports. Correlations were also performed to determine possible relationships among the different parameters.

Methods

A total of 8 fragments were collected from lower extremity long bones (femur or tibia) of 5 children with OI (sex: 2M, 3F; age range: 1.5-11.5 years) under written informed consent/assent and Institutional Review Board (IRB) approval during routine osteotomy surgical procedures (Shriners Hospitals for Children, Chicago, IL). All patients were diagnosed with moderate or severe OI (types IV or III, respectively), and 3 of the 5 patients had received at least one round of bisphosphonate therapy to increase bone mass. The specimens were stored in a freezer at -70°C prior to scanning. The bone fragments were scanned using the Keck micro-CT system described previously. Specimens were thawed and scanned in saline in continuous mode (33 kVp, 231 μA, 360 views, 7-frame average) to obtain 35-μm isotropic voxel resolution. As a preprocessing step, a ring artifact reduction algorithm was implemented on the projection images prior to reconstruction to decrease artifacts caused by detector limitations and to improve the ability of the segmentation procedure to correctly isolate the bone from its surroundings.[40] After the data was reconstructed with a Feldkamp algorithm, attenuation intensity values were converted to Hounsfield units (HU). Trabecular VOIs were identified from the resulting grayscale image volumes and analyzed for several structural parameters in MicroView (v2.1.2; GE Healthcare, Waukesha, WI). Cubic VOIs (2-mm side length) were segmented by applying a local threshold determined using the Auto-Threshold option in MicroView, which utilizes an Otsu cluster thresholding algorithm.[8] Each VOI was examined using the Bone Analysis tool, which directly measures BV/TV and BS/BV and then calculates Tb.Th, Tb.N, Tb.Sp, and Eu.Conn.D. Highly

connected tissues (such as healthy trabecular bone) have large, negative Euler numbers.

After the specimens were analyzed, 3-D surface-shaded renderings were produced using the MicroView Isosurface Tool for visualization purposes. BMD measurements are widely used for diagnostic purposes and evaluation and treatment efficacy.[3,5,10] We also performed several common bone densitometry measurements on the trabecular VOIs in MicroView including volumetric BMD, TMD, and BMC. BMC was calculated first by using a phantom (Image Analysis, Inc., Columbia, KY) with various hydroxyapatite (HA) concentrations (0, 75, and 150 mg-HA/cm^3) to convert the grey value (in HU) for each voxel in the VOI to an equivalent mass of mineral (in mg-HA). Volumetric BMD was then calculated by normalizing BMC by the total volume of the VOI. Finally, volumetric TMD was calculated by summing the BMC of only those voxels whose grey values were above a minimum bone threshold, then normalizing by the volume of all included voxels (Figure 2). This ensures exclusion of non-bone background material (e.g., air, water, marrow), which can greatly affect density calculations.

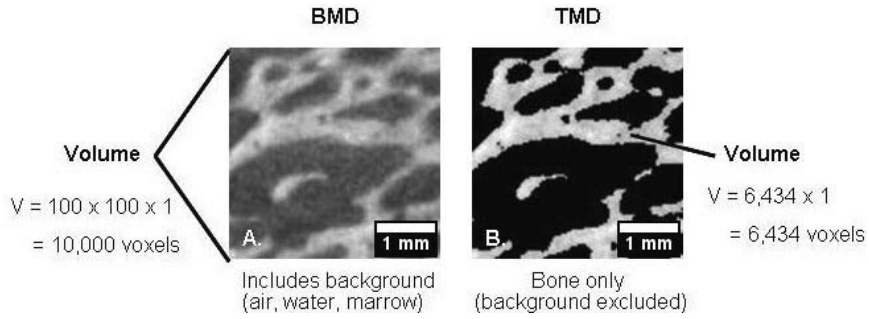

Figure 2. Description of methods applied to calculate BMD and TMD. A: All voxels are used for BMD, and the calculation is independent of any threshold; B: Only voxels with grey values greater than or equal to the bone threshold are counted in the calculation.

Results

General Morphology

Visualization of the rendered VOIs demonstrated that the trabeculae had general plate-like structure, common for lower extremity long bones (Figure 3). Unlike healthy bone, the OI trabecular plates did not appear to display a preferential orientation, suggesting less organized architectural characteristic, as is sometimes observed in diseased or deteriorating

cancellous bone structures, such as due to aging.[14] Samples from one of the severe (type III) OI patients appeared to follow characteristics found in the parallel plate bone model (Figure 3, G-H). Structural changes due to factors such as drug treatment, harvest site, gender, and OI (genetic) type were not evident or easily distinguishable.

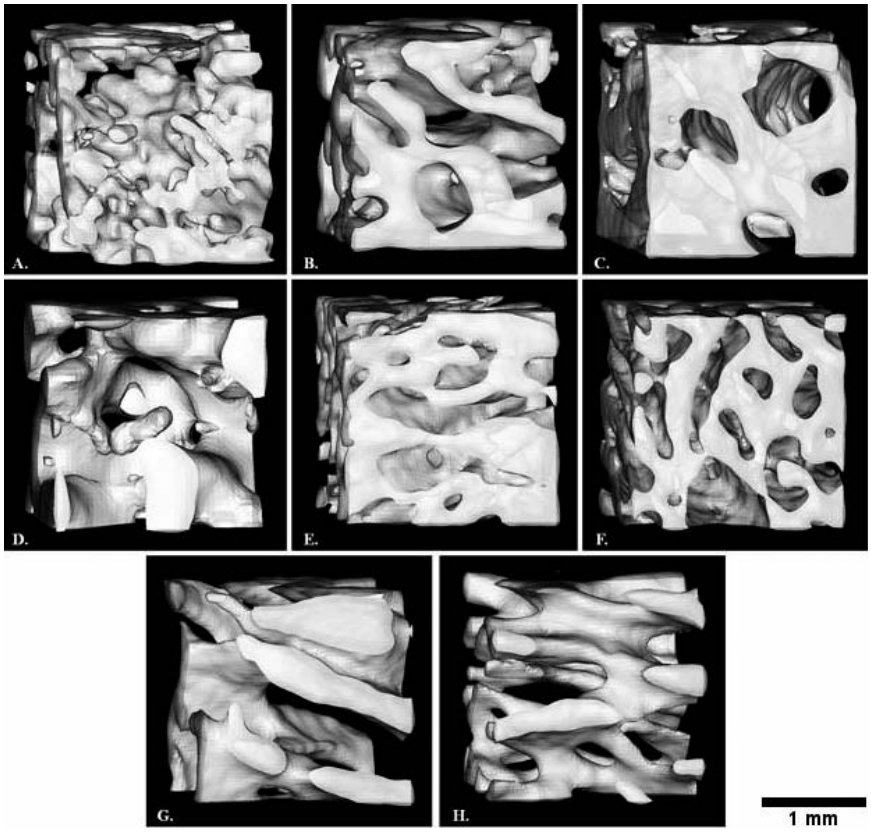

Figure 3. Surface-shaded renderings of trabecular VOIs. A*: Patient 1 (specimen 1-A, female, 8 yrs, type IV, tibia); B*: Patient 1 (specimen 1-B); C*: Patient 2 (specimen 2, female, 6.5 yrs, type III, tibia); D: Patient 3 (specimen 3, male, 10.5 yrs, type III, tibia); E*: Patient 4 (specimen 4-A, female, 1.5 yrs, type III/IV moderate, femur); F*: Patient 4 (specimen 4-B, 1.8 yrs, tibia); G: Patient 5 (specimen 5-A, male, 11.5 yrs, type III, femur). H: Patient 5 (specimen 5-B). *Indicates patient received bisphosphonate treatment.

Bone Morphometry

Results from the structural analysis are summarized in Table 3. Although parameters tended to display moderate heterogeneity across the sample population, both Eu.Conn.D and Tb.N were highly correlated with each other

(R^2=0.81) and these parameters tended to be related to severity of OI (R^2=0.51 and 0.50, respectively). Type III specimens also tended to have fewer trabeculae and lower connectivity than those from either type IV or III/IV patients. Several indices including BV/TV, Tb.N, and Eu.Conn.D were elevated in specimens from patients who had received at least one round of a bisphosphonate prior to harvesting. One patient who received such treatments between the first (4-A) and second (4-B) specimen collections exhibited modest increases in BV/TV and Tb.Th, but decreases in the other parameters.

Table 3. Bone morphometric parameters.

Specimen	OI type	BV/TV	BS/BV (1/mm)	Tb.Th (mm)	Tb.N (1/mm)	Tb.Sp (mm)	Eu.Conn.D ($1/mm^3$)
1-A*	IV	0.41	13.54	0.15	2.77	0.21	21.74
1-B*	IV	0.48	9	0.22	2.18	0.24	7.98
2	III	0.64	5.6	0.36	1.78	0.2	4.86
3*	III	0.43	8.34	0.24	1.79	0.32	7.13
4-A*	III/IV	0.41	14.52	0.14	2.98	0.2	18.02
4-B*	III/IV	0.58	9.35	0.21	2.73	0.15	10.78
5-A	III	0.28	9.37	0.21	1.33	0.54	1.84
5-B	III	0.26	13.19	0.15	1.74	0.42	3.84
Median (range):		0.42 (0.37)	9.36 (8.92)	0.21 (0.22)	1.99 (1.65)	0.23 (0.38)	7.56 (19.9)

*Patient received bisphosphonate treatment prior to specimen harvesting.

BMD

Results from the BMD tests are summarized in Table 4. This analysis did not reveal any clear relationships between OI severity and bone mineral metrics. Yet, patients who received drug therapy tended to have increased BMD and BMC compared to untreated peers, and like the results of the structural analysis, the patient who underwent drug treatment between specimen collections exhibited substantial increases in all mineral parameters (Table 4, specimens 4-A and 4-B).

Table 4. BMD calculations.

Specimen	OI Type	BMD (mg/cm^3)	TMD (mg/cm^3)	BMC (mg)
1-A*	IV	232.3	564.6	1.87
1-B*	IV	411.6	831.2	3.25
2	III	558.1	868.3	4.48
3*	III	400.0	907.3	1.36
4-A*	III/IV	278.6	661.9	2.24
4-B*	III/IV	470.6	806.8	3.78
5-A	III	228.9	791.4	1.84
5-B	III	200.8	759.2	1.61
Median (Range):		339.3 (357.2)	799.1 (342.7)	2.05 (3.13)

*Patient received bisphosphonate treatment prior to specimen harvesting.

Discussion

Several historic studies have used standard histomorphometric methods to examine small OI populations,[41-43] however, there is surprisingly little data on how OI affects bone and its development. While McCarthy et al.[42] focused on adult populations and the Baron and Ste-Marie studies tested relatively small clinical populations (n<10), Rauch et al., in the most extensive study to date, used histomorphometric methods to characterize bone specimens from 70 children with OI and 27 age-matched controls.[44] The Rauch study, in which individuals having undergone pharmacological therapy were excluded, found significantly decreased BV/TV, Tb.N, and Tb.Th in individuals with OI and minimal differences in trabecular parameters between types III and IV in the OI population.

In our current study, Micro-CT was used to quantitate measures of trabecular microstructure and mineralization in pediatric bone specimens from children with a range of moderate to severe OI. Morphometric indices determined were generally higher than those reported in the histomorphometric studies. These differences may be explained by the following factors. These previously published histological studies tested bone biopsies from the iliac crest, while specimens in the current study were collected from lower extremity long bones. As previous mentioned, histological studies rely on model assumptions to extrapolate structural 3-D parameters from thin 2-D specimens. These limitations can lead to more

conservative parameter estimates. Furthermore, most of the specimens in our study came from patients who also received drugs targeted to enhance bone mass, effectively increasing indices. These drugs affect bone structure and mineral composition. Our analysis was able to detect the augmented effects despite a small sample size.

One interesting observation from our study was that Eu.Conn.D and Tb.N were highly correlated and related to the severity of OI. Detecting differences in these indices could prove to be important differential diagnostic procedure for assessment and distinguishing OI types. As an example, although one of the patients within the study was diagnosed with type III/IV OI based on clinical observations, indices determined through micro-CT analysis suggest the patient's bone characteristics are more similar to other type IV patients.

Simple linear regression analyses suggest strong correlations between the morphometric and mineral parameters (Figure 4). The strongest structural correlations occurred between BMD, TMD, and BMC with BV/TV, BS/BV, and BV/TV, respectively. The finding that BV/TV was strongly related to two mineral content parameters underscores the importance of considering both structure and bone mass when analyzing trabecular bone.[3,45]

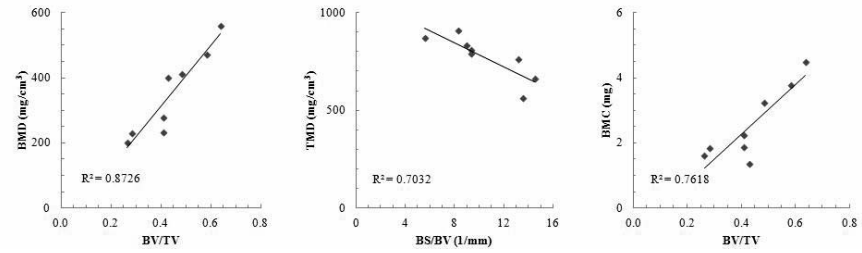

Figure 4. Correlations between architectural and mineral parameters.

The results of the current study present some of the first quantitative micro-CT data on human OI bone, and provide intriguing evidence for the use of micro-CT analysis in OI bone. Nonetheless, we must acknowledge factors that potentially confound the study. These include the fact that specimens tested came from different sites within femora and tibia and the exact site of excision was not rigorously documented.

FUTURE OF BONE QUANTIFICATION AND CHARACTERIZATION OF OI

With the advent of high-resolution micro-CT systems available for clinical evaluation and research, *in vivo* scanning of OI may become a valuable clinical tool. To achieve this, several technical challenges must be addressed. These challenges include improving algorithms to more systematically and/or automatically determine the volume of interest, minimizing radiation dose (a goal more broadly addressed by projects like that found at imagegently.org and imagewisely.org), and developing applicable standardized imaging protocols to address consistency and repeatability. Current scanners allow for the examination of extremitie,[35-38] which may be ideal for evaluation and analysis of OI patients with symptomatic expression in legs or arms, however, with the current geometry of the scanners relatively proximal scans are likely to be difficult if not impossible. Unfortunately, the use of orthopedic hardware such as screws and rods in the clinical management of OI cause image artifacts that complicate and in some cases undermine the use of CT imaging and analysis methods. New techniques for removing these artifacts will be required to avoid this practical drawback.

Fragments of bone that are excised through surgical intervention for correcting deformities will still be available for *ex vivo* research and analysis, but a more likely scenario is that presurgical *in vivo* scanning will have already been performed for bone assessment and pre-operative planning.

The current state of fracture risk assessment and bone biomechanical models, especially those in OI or that incorporate structural and material properties measured through imaging, is still in its relative infancy.[1-4,6,27,46] Methods and protocols for maintaining consistent imaging geometries and analytical techniques require standardization and optimization. In addition, more studies in which intact bones are imaged, modeled, and mechanically tested are greatly needed. Finite element analysis techniques derived from micro-CT data are also likely to become chief methods of bone analysis.[1,10,47] The biomechanical competence of bone is a function of its geometrical and material properties. Links between bone microstructure, composition, and mechanical characteristics are recently becoming better understood.[1-3,5,10] Increasingly it is becoming evident that bone strength and risk of fracture is only partially determined by bone mineralization and that bone architecture has considerable influence.

Currently, the technique of analyzing volumetric imaging data is relatively tedious and requires substantial computer processing capacity. Automated algorithms and protocols must be developed to improve throughput, reproducibility, and to reduce user bias that is inherently introduced. With some semi-automated techniques becoming available, such as those found in BoneJ (a plug-in for the open source image processing software platform ImageJ),[48] consensus on standards for analytical implementations are sure to soon follow.

Although not practical for *in vivo* or clinical use, synchrotron source micro-CT[1,7,49-51] provides advantages over standard X-ray micro-CT, such as higher spatial resolution, alternative contrast techniques, fewer artifacts, and a nearly monochromatic energy source, driving research that aims to better understand and characterize minute bone features and more precise distribution of material composition. With its superior resolution, synchrotron source imaging applied to bone will aid in the assessment of microdamage, capturing features such as the orientation and geometry of microcracks and secondary osteon, that plays a role in initiating or dissipating energy and regulating the repair process, ultimately impacting bone quality and fracture healing.

Recent advances in micro-CT imaging, morphometric analysis, and biomechanical modeling are creating new opportunities to study and understand bone biology, architecture, fracture risk, and the effects of pharmacotherapy. These combined methods are gaining more widespread acceptance and are quickly becoming incorporated into clinical trials. Although currently the techniques entail specialized equipment, exposure to modest amounts ionizing radiation, and require non-standardized image analysis, they provide information about BMD, macrostructure, and microstructure. Furthermore, there is a high likelihood that these technical limitations will soon be reduced or eliminated. Advanced techniques in micro-CT, FEM, and bone modeling are certainly poised to improve our understanding of bone biomechanics, fracture propensity, and clinical management of OI.

ABBREVIATIONS

2-D	Two-dimensional
3-D	Three-dimensional
+ -	Wild-type
BMD	Bone mineral density
CCD	Charge-coupled device
cm	Centimeter
CT	Computed tomography
DEXA	Dual-energy X-ray absorptiometry
FEM	Finite element method
GE	General Electric
HA	Hydroxyapatite
HU	Hounsfield units
keVs	Kiloelectron-volts
kVp	Peak kilovoltage
OI	Osteogenesis imperfecta
oim	Osteogenesis imperfecta murine (mouse) model
mg	Milligram
micro-CT	Micro-computed tomography
mL	Milliliter
mm	Millimeter
NIH	National Institutes of Health
ROI	Region of interest
uA	Microamp
uL	Microliter
um	Micrometer
VOI	Volume of interest
voxel	Volume element

REFERENCES

1. Ito M. Assessment of bone quality using micro-computed tomography (micro-CT) and synchrotron micro-CT. *J. Bone Miner. Metab.* 2005; 23 Suppl: 115-21.
2. Liebschner MA, Muller R, Wimalawansa SJ, et al. Testing two predictions for fracture load using computer models of trabecular bone. *Biophys. J.* 2005; 89(2): 759-67.
3. Jiang Y, Zhao J, Liao EY, et al. Application of micro-CT assessment of 3-D bone microstructure in preclinical and clinical studies. *J. Bone Miner. Metab.* 2005; 23 Suppl: 122-31.
4. Yeni YN, Brown CU, Wang Z, et al. The influence of bone morphology on fracture toughness of the human femur and tibia. *Bone*. 1997; 21(5): 453-9.

5. Ito M, Ikeda K, Nishiguchi M, et al. Multi-detector row CT imaging of vertebral microstructure for evaluation of fracture risk. *J. Bone Miner. Res.* 2005; 20(10): 1828-36.
6. Engelke K, Song SM, Gluer CC, et al. A digital model of trabecular bone. *J. Bone Miner. Res.* 1996; 11(4): 480-9.
7. Bouxsein ML, Boyd SK, Christiansen BA, et al. Guidelines for assessment of bone microstructure in rodents using micro-computed tomography. *J. Bone Miner. Res.* 2010; 25(7): 1468-86.
8. Sezgin M, Sankur B. Survey over image thresholding techniques and quantitative performance evaluation. *J. Electron. Imaging.* 2004; 13(1): 146-65
9. Muller R, Van Campenhout H, Van Damme B, et al. Morphometric analysis of human bone biopsies: a quantitative structural comparison of histological sections and micro-computed tomography. *Bone*. 1998; 23(1): 59-66.
10. Genant HK, Engelke K, Prevrhal S. Advanced CT bone imaging in osteoporosis. *Rheumatology* (Oxford). 2008; 47 Suppl 4: iv9-16.
11. Ito M, Nishida A, Nakamura T, et al. Differences of three-dimensional trabecular microstructure in osteopenic rat models caused by ovariectomy and neurectomy. *Bone*. 2002; 30(4): 594-8.
12. Ito M, Nakamura T, Matsumoto T, et al. Analysis of trabecular microarchitecture of human iliac bone using microcomputed tomography in patients with hip arthrosis with or without vertebral fracture. *Bone*. 1998; 23(2): 163-9.
13. Muller R, Ruegsegger P. Three-dimensional finite element modelling of non-invasively assessed trabecular bone structures. *Med. Eng. Phys.* 1995; 17(2): 126-33.
14. Hildebrand T, Ruegsegger P. Quantification of Bone Microarchitecture with the Structure Model Index. *Comput Methods Biomech Biomed Engin.* 1997; 1(1): 15-23.
15. Fung YC. Mechanical properties of living tissues. *Biomechanics*. New York: Springer-Verlag; 1993. p. 500-36
16. Pereira R, Khillan JS, Helminen HJ, et al. Transgenic mice expressing a partially deleted gene for type I procollagen (COL1A1). A breeding line with a phenotype of spontaneous fractures and decreased bone collagen and mineral. *J. Clin. Invest.* 1993; 91(2): 709-16.
17. Chipman SD, Sweet HO, McBride DJ, Jr., et al. Defective pro alpha 2(I) collagen synthesis in a recessive mutation in mice: a model of human osteogenesis imperfecta. *Proc. Natl. Acad. Sci. USA.* 1993; 90(5): 1701-5.
18. Bonadio J, Saunders TL, Tsai E, et al. Transgenic mouse model of the mild dominant form of osteogenesis imperfecta. *Proc. Natl. Acad. Sci. USA.* 1990; 87(18): 7145-9.
19. Camacho NP, Hou L, Toledano TR, et al. The material basis for reduced mechanical properties in oim mice bones. *J. Bone Miner. Res.* 1999; 14(2): 264-72.
20. Gasser JA, Ingold P, Grosios K, et al. Noninvasive monitoring of changes in structural cancellous bone parameters with a novel prototype micro-CT. *J. Bone Miner. Metab.* 2005; 23 Suppl: 90-6.
21. Karau KL, Johnson RH, Molthen RC, et al. Microfocal X-ray CT imaging and pulmonary arterial distensibility in excised rat lungs. *Am J Physiol Heart Circ Physiol.* 2001; 281(3): H1447-57.
22. Karau KL, Molthen RC, Dhyani A, et al. Pulmonary arterial morphometry from microfocal X-ray computed tomography. *Am J Physiol Heart Circ Physiol.* 2001; 281(6): H2747-56.

23. Molthen RC, Karau KL, Dawson CA. Quantitative models of the rat pulmonary arterial tree morphometry applied to hypoxia-induced arterial remodeling. *J. Appl. Physiol.* 2004; 97(6): 2372-84; discussion 54.
24. Feldkamp LA, DAVIS LC, KRESS JW. Practical cone-beam algorithm. *Journal of the Optical Society of America A.* 1984; 1(6): 612-9.
25. Misof BM, Roschger P, Baldini T, et al. Differential effects of alendronate treatment on bone from growing osteogenesis imperfecta and wild-type mouse. *Bone*. 2005; 36(1): 150-8.
26. Uveges TE, Kozloff KM, Ty JM, et al. Alendronate treatment of the brtl osteogenesis imperfecta mouse improves femoral geometry and load response before fracture but decreases predicted material properties and has detrimental effects on osteoblasts and bone formation. *J. Bone Miner. Res.* 2009; 24(5): 849-59.
27. McBride DJ, Jr., Shapiro JR, Dunn MG. Bone geometry and strength measurements in aging mice with the oim mutation. *Calcif. Tissue Int.* 1998; 62(2): 172-6.
28. Muller R, Hahn M, Vogel M, et al. Morphometric analysis of noninvasively assessed bone biopsies: comparison of high-resolution computed tomography and histologic sections. *Bone.* 1996; 18(3): 215-20.
29. Interdisciplinary treatment approach for children with osteogenesis imperfecta. Chiasson RM, Munns C, Zeitlin L, editors: Shriners Press; 2004.
30. Petit MA, Beck TJ, Kontulainen SA. Examining the developing bone: What do we measure and how do we do it? *J Musculoskelet Neuronal Interact.* 2005; 5(3): 213-24.
31. Fan ZF, Smith P, Rauch F, et al. Nanoindentation as a means for distinguishing clinical type of osteogenesis imperfecta. *Composites Part B: Engineering.* 2007; 38(3): 411–5.
32. Fan Z, Smith PA, Harris GF, et al. Comparison of nanoindentation measurements between osteogenesis imperfecta Type III and Type IV and between different anatomic locations (femur/tibia versus iliac crest). *Connect. Tissue Res.* 2007; 48(2): 70-5.
33. Fan Z, Smith PA, Eckstein EC, et al. Mechanical properties of OI type III bone tissue measured by nanoindentation. J Biomed Mater Res A. 2006; 79(1): 71-7.
34. Kalpakcioglu BB, Morshed S, Engelke K, et al. Advanced imaging of bone macrostructure and microstructure in bone fragility and fracture repair. *J. Bone Joint Surg. Am.* 2008; 90 Suppl 1: 68-78.
35. Firoozabadi R, Morshed S, Engelke K, et al. Qualitative and quantitative assessment of bone fragility and fracture healing using conventional radiography and advanced imaging technologies--focus on wrist fracture. *J. Orthop. Trauma.* 2008; 22(8 Suppl): S83-90.
36. Boutroy S, Bouxsein ML, Munoz F, et al. In vivo assessment of trabecular bone microarchitecture by high-resolution peripheral quantitative computed tomography. *J. Clin. Endocrinol. Metab.* 2005; 90(12): 6508-15.
37. Khosla S, Melton LJ, 3rd, Achenbach SJ, et al. Hormonal and biochemical determinants of trabecular microstructure at the ultradistal radius in women and men. *J. Clin. Endocrinol. Metab.* 2006; 91(3): 885-91.
38. Burghardt AJ, Issever AS, Schwartz AV, et al. High-resolution peripheral quantitative computed tomographic imaging of cortical and trabecular bone microarchitecture in patients with type 2 diabetes mellitus. *J. Clin. Endocrinol. Metab.* 2010; 95(11): 5045-55.
39. Jameson J, Albert C, Molthen R, et al., editors. Micro-CT characterization of human trabecular bone in osteogenesis imperfect. *Medical Imaging: Biomedical*

Applications in Molecular, Structural, and Functional Imaging; 2011 February 13-17, 2011; Lake Buena Vista, FL: SPIE, Bellingham, WA.
40. Rivers. M. L., Sutton S. Geoscience applications of X-ray computed microtomography. *Proceedings of SPIE*, Developments in X-ray Tomography II. 1999; 3772: 78-86.
41. Baron R, Gertner JM, Lang R, et al. Increased bone turnover with decreased bone formation by osteoblasts in children with osteogenesis imperfecta tarda. *Pediatr. Res.* 1983; 17(3): 204-7.
42. McCarthy EF, Earnest K, Rossiter K, et al. Bone histomorphometry in adults with type IA osteogenesis imperfecta. *Clin Orthop Relat Res*. 1997; (336): 254-62.
43. Ste-Marie LG, Charhon SA, Edouard C, et al. Iliac bone histomorphometry in adults and children with osteogenesis imperfecta. *J. Clin. Pathol.* 1984; 37(10): 1081-9.
44. Rauch F, Travers R, Parfitt AM, et al. Static and dynamic bone histomorphometry in children with osteogenesis imperfecta. *Bone*. 2000; 26(6): 581-9.
45. Cointry GR, Capozza RF, Chiappe MA, et al. Novel experimental effects on bone material properties and the pre- and postyield behavior of bones may be independent of bone mineralization. *J. Bone Miner. Metab.* 2005; 23 Suppl: 30-5.
46. Yeni YN, Brown CU, Norman TL. Influence of bone composition and apparent density on fracture toughness of the human femur and tibia. *Bone*. 1998; 22(1): 79-84.
47. Dragomir-Daescu D, Op Den Buijs J, McEligot S, et al. Robust QCT/FEA models of proximal femur stiffness and fracture load during a sideways fall on the hip. *Ann. Biomed. Eng.* 2011; 39(2): 742-55.
48. Doube M, Klosowski MM, Arganda-Carreras I, et al. BoneJ: Free and extensible bone image analysis in ImageJ. *Bone*. 2010; 47(6): 1076-9.
49. Larrue A, Rattner A, Peter ZA, et al. Synchrotron radiation micro-CT at the micrometer scale for the analysis of the three-dimensional morphology of microcracks in human trabecular bone. *PLoS One.* 2011; 6(7): e21297.
50. Cooper DM, Erickson B, Peele AG, et al. Visualization of 3D osteon morphology by synchrotron radiation micro-CT. *J. Anat.* 2011; 219(4): 481-9.
51. Matsumoto T, Nishikawa K, Tanaka M, et al. In vivo CT quantification of trabecular bone dynamics in mice after sciatic neurectomy using monochromatic synchrotron radiation. *Calcif. Tissue Int.* 2011; 88(5): 432-41.